4th International Conference on
Structural Health Assessment of Timber Structures
20-22 September 2017 Istanbul, Turkey

ASSESSMENT OF THE *JUPITER JOINT*'S IN-PLANE AND OUT-OF-PLANE MECHANICAL BEHAVIOR UNDER COMBINED ACTIONS.

E. Perria[1], M. Kessel[1], M. Paradiso[2], M. Sieder[1]

[1] iBHolz, Institut für Baukonstruktion und Holzbau, Technische Universität Braunschweig

[2] DIDA, Dipartimento di Architettura, Università degli studi di Firenze

Keywords: Historical Timber, Woodwork joints, Jupiter joint, Structural Analysis

Abstract.

Introduction:

Old timber structures are characterized by the complexity of structural elements and joints. The understanding of the basic working principles of the structural elements and joints is of basic importance for the definition of the load-carrying capacity and stiffness of the whole structure. Comprehensive and detailed information regarding design rules for the assessment and characterization of the carpentry joints are missing in the current scientific literature.

Developments:

The paper presents experimental results on the behavior of the Jupiter joint (stop-splayed undersquinted & tabled with key joint), one among the most diffused elongation scarf joints. The tests are done on specimens with a specific geometry with inclination of the connecting surfaces of $\alpha = 60°$ and $\beta = 5°$ [Fig. 3]. Experimental in-plane and out-of-plane tests are proposed. The joint is loaded under external actions of pure compression, pure bending and combined compressive and bending stress. The failure modes and the qualitative influence of the geometry on the load-carrying capacity of the joint are described in detail. The paper concludes with the quantitative evaluation of the load-carrying capacity along both the strong and weak axis of the joint, expressed in min values, and represented in a N-M interaction diagram (pairs of normal force N and bending moment M).

Remarks and Conclusion:

The paper contains useful upgrades in the evaluation of carpentry connections' mechanical properties, more specifically in the field of the scarf joints. Useful pieces of information for the structural analysis of traditional timber constructional systems are presented.

1. INTRODUCTION

Timber historical buildings are diffused in many regions of the world. They are essential to the landscape of cities and countries, and constitute a precious example of both tangible and intangible historical heritage. For this reason, their maintenance and restoration is of basic importance. Nevertheless, historical buildings deserve particular attention at the moment of the intervention. In fact, old timber structures are characterized by the complexity of structural elements and joints. The understanding of the basic principles under which the structure works, is of basic importance for the definition of the correct restoration and strengthening work.

The carpentry structures and the joinery techniques are the result of a long-term process of evolution along the centuries and present a variety of constructional techniques that significantly vary according to regional building traditions. More than 600 different geometries of carpentry joints are known, and there are so many constructive techniques than cultures. According to the task they have to fulfill in the timber structure, the joints can be divided in different categories: lengthening, bearing, framing, angle and oblique shouldered joints. Among the most diffuse lengthening joint, the *stop-splayed undersquinted and tabled with key scarf* joint, also called *Jupiter joint*, has the function to enlarge the beams and other timbers along their longitudinal direction.

In the present paper, the load-bearing behavior and deformation behavior of the *Jupiter joint* carpentry connection, as found in historical wooden structures, is investigated.

1.1. Goals

The main aims pursued in the present paper are:

- Experimental evaluation of the load-carrying capacity of the *Jupiter joint* under combined compressive and bending action.
- Evaluation of the in-plane and out-of-plane behavior of the *Jupiter joint* under combined compressive and bending action.
- Representation of the experimental load-carrying capacity with a N-M interaction diagram (diagram that describes the interaction between normal force N and bending moment M).
- Evaluation of the failure modes for both the in-plane and out-of plane load directions.
- Quantification of the rotational stiffness' values to use in both the practice and structural analysis simulation.

1.2. Methodology

The adopted methodology is the scientific method. It consists of developed theories, systematic tests, measurements, observations, and modification of the initially adopted hypotheses. The adopted approach in this paper is experimental. The work consists of static in-plane and out-of-plane tests on scaled timber beams. The tests were carried out during the period April 2015 - July 2016, in the LHT Laboratory for wooden technology of the Faculty Building and Preserving in the HAWK Hildesheim (University of applied sciences), Germany.

2. MATERIAL AND METHODS

2.1. Equipment

The used machinery is Walter+Bai ag. (for forces up to $F_{c,max} = 250$ kN and $F_{t,max} = 160$ kN) controlled by a desktop computer with software Proteus. The equipment consists in the combination of two subsystems, two hydraulic jacks, one for vertical and the other for the horizontal loads. The Piston I is used for the application of axial forces ($F_{applied} = F_I$) and the Piston II for the application of bending moment ($F_{applied} = F_{II}$) (see equation (2) for the relation between applied force F_{II} and moment M). The force is exerted on the test specimens by means of movable cross-heads fixed to the frame. The head of the Piston II is provided with a head for the application of bending moment to the specimens.

2.2. Procedures

The procedure 2 tests (P2) follow a mixed force-controlled and displacement-controlled mode procedure. The P2 is described by the separate and consecutive loading of specimens by the Piston I and Piston II on the specimen's strong axis (Figure 1). The load F_I increases with force-controlled mode up to the chosen value of F_{target}; afterwards, the F_{II} with displacement-controlled mode is applied until the specimen's failure. During the loading the forces F_I and F_{II} and the correspondent pistons displacements w_I and w_{II} are measured. The relation among F_I force and the normal force (N) is defined in the equation (1). The one among the applied F_{II} force and the bending moment (M) by the equation (2).

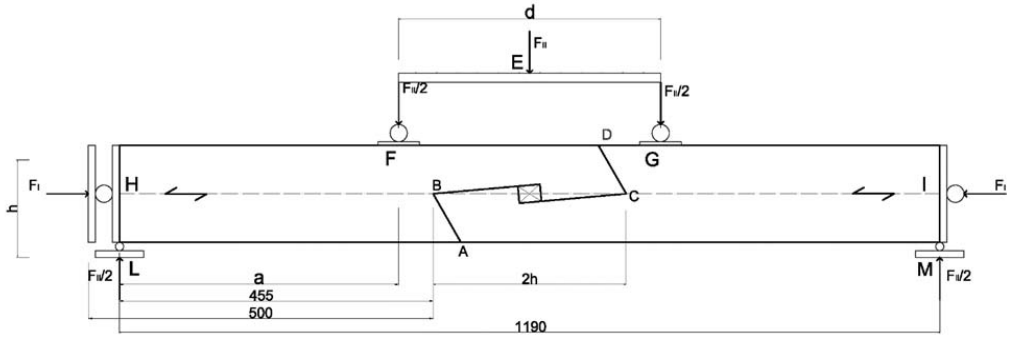

Figure 1: P2 tests asset for the application of compressive and bending force on the strong axis. All the dimensions are expressed in [mm]

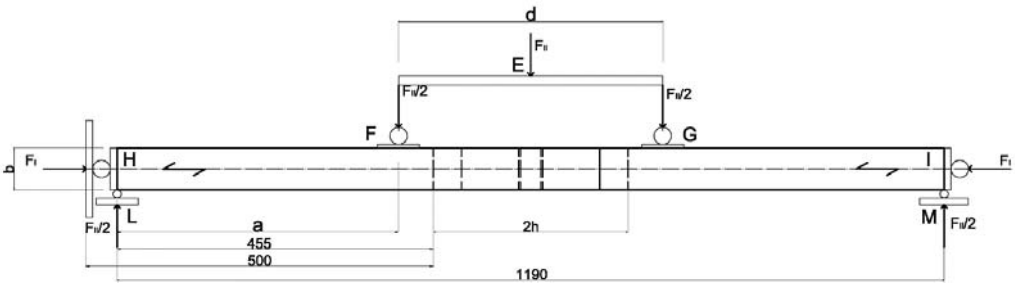

Figure 2: P3 tests asset for the application of compressive and bending force on the weak axis. All the dimensions are expressed in [mm]

The procedure 3 tests (P3) follow a mixed force-controlled and displacement-controlled mode procedure. The P3 is analogous to the Procedure 2, but the specimens are turned 90° and tested along the weak axis (Figure 2). The relation among F_I force and the normal force (N) is defined in the following equation (1). The one among the applied F_{II} force and the bending moment (M) by the equation (2).

$$N = F_I \qquad [kN] \tag{1}$$

$$M = \frac{F_{II}}{2} \cdot a \qquad [kN \cdot mm] \tag{2}$$

Where:

$$\begin{cases} a = 405\,mm & for \quad P1, P2 \\ a = 390\,mm & for \quad P3 \end{cases} \tag{3}$$

2.3. Specimens

The specimens are prepared from artificially dried solid timber beams of length 650 cm with a cross-section of b = 60 mm, h = 140 mm. The wood specie is spruce (*Picea abies*), timber strength class C24. The specimens are stored at a temperature of 20° C with relative humidity of 65%.

The specimen 6 (S6) is prepared for the analysis of the *Jupiter joint* along the strong and weak axis (Figure 3). The specimen surfaces are inclined of $\alpha = 60°$ and $\beta = 5°$. The joint is provided with a square-cut key.

The specimens' preparation consists of two different montages in the machinery according to the below described procedures.

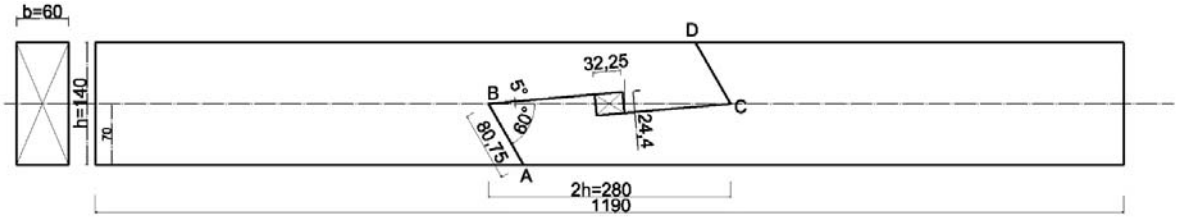

Figure 3: Specimen S6. Specimen used for the tests of the *Jupiter joint*. All the dimensions are in [mm]

3 TESTS

3.1 Strong axis tests

In Figure 4 are pictured the N-M interaction curves (interaction between the normal force N and the bending moment M) for the *Jupiter joint* (*stop-splayed undersquinted and tabled with key* scarf joint). The curves are the interpretation of the individual performed test results [1]. The strong axis tests are represented in colored results, while the weak axis tests are in bolt. The red line represents the strong axis' load-bearing interaction curve. The specimens are S6, performed with P2. The violet line describes the weak axis' load-bearing interaction curve. All the tests specimen are S6, and performed with P3.

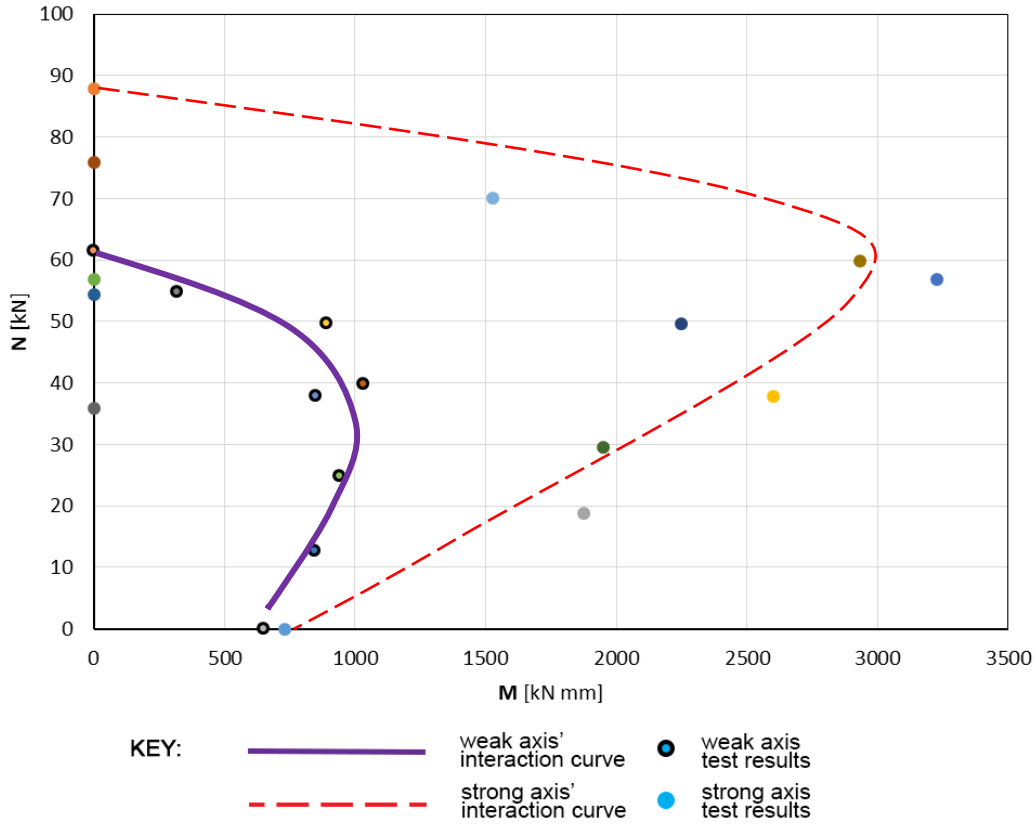

Figure 4: N-M interaction diagram for the *Jupiter joint* along the strong and weak axis

3.1.1 Failure modes (FM)

The failure modes observed in the weak axis' tests are mainly three, and are described as:

- FM II. Shear/tension perpendicular to the grain failure in the point B
- FM III Combined shear/tension perpendicular to the grain failure in the points B and C
- FM V. Shear failure in the BB''C'H prism.

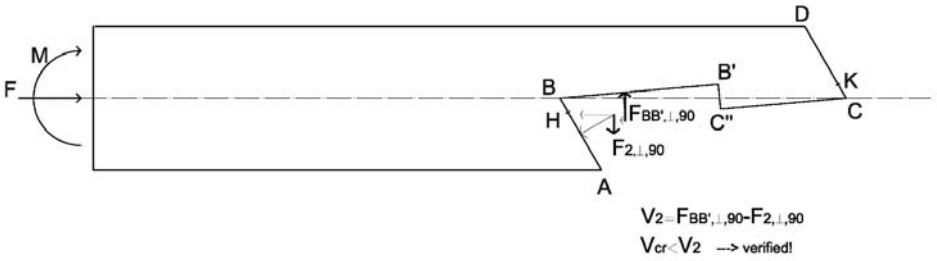

Figure 5: FM II. Shear/ tension perpendicular to the grains failure, active forces

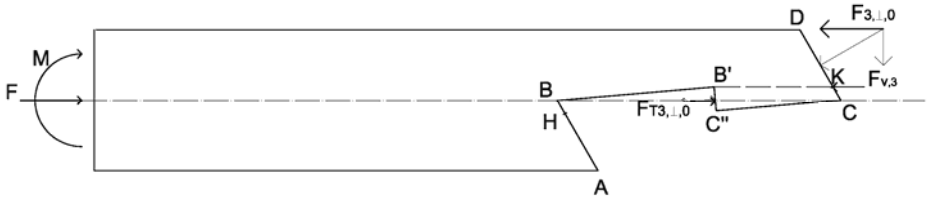

Figure 6: FM V Shear failure in the BB''C'H prism, active forces

FM I	FM II	FM III	FM IV	FM II + FM V	FM V
(…)			(…)		
	(a)	*(b)*		*(c)*	*(d)*

Figure 7: Failure mode of specimens of *Jupiter joint*, in-plane testing: (a): Specimen J60_5_S_F76_M α = 60° β = 5° 19/07/2016 compression force. (b): Specimen J60_5_S_F65_M α = 60° β = 5° 19/07/2016 compression force. (c): Specimen J60_5_S_F19_M α = 60° β = 5° 19/07/2016 compression and bending force. (d): Specimen J60_5_S_F0 α = 60° β = 5° 18/07/2016 pure bending

For all the specimens loaded along the strong axis, the main failure modes are the FM II and the combination of FM II and FM V. The failure modes are resumed in the Figure 7.

Referring to the Figure 6, the FM V is the shear failure in the lower timber piece's BB''C'H prism, for the whole depth *b* of the beam, and FM II happens in the lower timber piece along the fibers in correspondence of the point B, also for the whole depth *b* of the beam. It follows a more detailed description of the active forces on the surfaces that cause the failure.

FM II: The plain mechanism of fracture FM II on the compression and tension side is explained in the Figure 5. The failure is due to the contemporary action of the forces V_2 and V_{cr}:

$$\begin{aligned} V_2 &= F_{BB',\perp,90} - F_{2,\perp,90} \\ V_{cr} &\geq V_2 \rightarrow \textit{failure} \end{aligned} \tag{4}$$

FM V: The shear failure is present both on the tensile and compressed side. The shear mechanism develops on the $\overline{B'K}$ shear plane. According to Figure 6, the shear force $F_{v,3}$ is dependent on the $F_{T3,0}$ and the $F_{3,\perp,0}$. The shear force acting on the shear plane $\overline{B'K}$ is:

$$F_{v,3} = F_{3,\perp,0} - F_{T3,\perp,0} \tag{5}$$

The section is verified when:

$$\frac{F_{v,3}}{b \cdot \overline{B'K}} \leq R_v \tag{6}$$

where: F_{pc} = pre - compression force; $F_{B'C'',\perp}$ = resultant force on the $\overline{B'C''}$ surface due to the external load, perpendicular to the surface; $F_{T3,\perp}$ = resultant force on the table 3 (T3 = surface $\overline{B'C''}$) of the joint, perpendicular to the surface; $F_{3,\perp}$ = resultant force on the face $\overline{DC}$ due to the external applied load, perpendicular to the surface; and $F_{T3,\perp,0} = F_{B'C'',\perp,0} + F_{pc,0}$.

3.2 Weak axis tests

The N-M interaction curve for the *stop-splayed undersquinted and tabled with key scarf* joint loaded along the weak axis is represented by the violet curve in Figure 4.

3.2.1 Failure modes

The observed weak axis's failure modes are mainly three and are following described:

- FM II. Shear/tension perpendicular to the grain failure in the point B
- FM III. Combined shear/tension perpendicular to the grain failure in the points B and C
- FM V. Shear failure in the BB''C'HBB''C'H prism.

According to the upper specimen in the Figure 10, the compression side is characterized by points A, H, B, B', B'', C', C'', C, K, D; while the tension side is characterized by the points A, H, B, B', B'', C', C'', C, D. For the specimens loaded along the weak axis the prevalent failure modes are the FM II, followed by the FM IV. The failure modes in the compression side are reported in Figure 9, and the ones observed in the tension side are in Figure 8.

The FM V is the shear failure in the lower timber piece's BB''C'H<u>BB</u>''<u>C</u>'<u>H</u> prism (Figure 10). The FM II happens in the upper timber piece's point B. The FM III is considered as secondary and due to the presence of the imperfections in the wood. It follows a more detailed description of the active forces on the surfaces that cause the failures, basing on test results and some basic equilibrium rules. The problem of the failure is very complicated because it implies some internal kinematic mechanisms that are explained in Figure 10 and brings both to the FM II and FM V.

FM II: Referring to Figure 10 and Figure 11, the FM II is explained through some three dimensional diagrams that consider the variation of the forces in the cross–section and the relative developed kinematic mechanisms. Here:

a) Because of $F_{T2,\perp,90}$ force, the grains in B are tensile-stressed in the upward direction.

b) Because of $F_{2,\perp,90}$ on the tension side, the fibers in <u>B</u> are tensile-stressed in the downward direction.

c) Because of $F_{T2,\perp,90}$ and $F_{2,\perp,90}$ forces, the clockwise torque $M_{BHC'B''}$ forms along the longitudinal direction of the compression side. The torque brings to the additional compression of the facing $\overline{AB}$ and $\overline{BB''}$ surfaces on the compressed side.

d) The force $F_{2,\perp,90}$ on the tension side, together with the $F_{2,\perp,90}$ on the compression side, bring to the formation of the anticlockwise torque $M_{\underline{BH}BH}$. The torque brings to the torsion of the specimen along the neutral axis that causes a non-homogeneous distribution of the compression force in the squint AB<u>AB</u> (Figure 11).

Because of the kinematic mechanisms above descripted in a), b), c), d), the FM II develops both in B, on the compression side, and in <u>B,</u> on the tension side.

FM I	FM II	FM III	FM IV	FM II + FM V	FM V
(...)			(...)		
	(a)	(b)		(c)	(d)

Figure 8: Failure mode on the tension side of specimens of *Jupiter joint*; out-of-plane tests: (a): Specimen J60_5_w_F50_M α = 60° β = 5° 21/07/2016 compression and tension stress. (b): Specimen J60_5_w_F55_M α = 60° β = 5° 21/07/2016 compression and tension stress. (c): Specimen J60_5_w_F12_M α = 60° β = 5° 21/07/2016, compression and tension stress. (d): Specimen J60_5_w_F25_M α = 60° β = 5° 21/07/2016 compression and tension stress

FM I	FM II	FM III	FM IV	FM II + FM IV	FM V
(...)	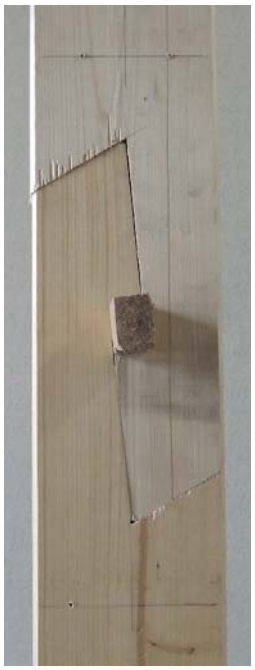		(...)		
	(a)	(b)		(c)	(d)

Figure 9: Failure modes on the compression side of specimens of *Jupiter joint*; out-of-plane tests: (a): Specimen J60_5_w_F50_M α = 60° β = 5° 21/07/2016 compression and tension stress. (b): Specimen J60_5_w_F55_M α = 60° β = 5° 21/07/2016 compression and tension stress. (c) Specimen J60_5_w_F38_M α = 60° β = 5° 21/07/2016, compression and tension stress. (d): Specimen J60_5_w_F12_M α = 60° β = 5° 21/07/2016 compression and tension stress

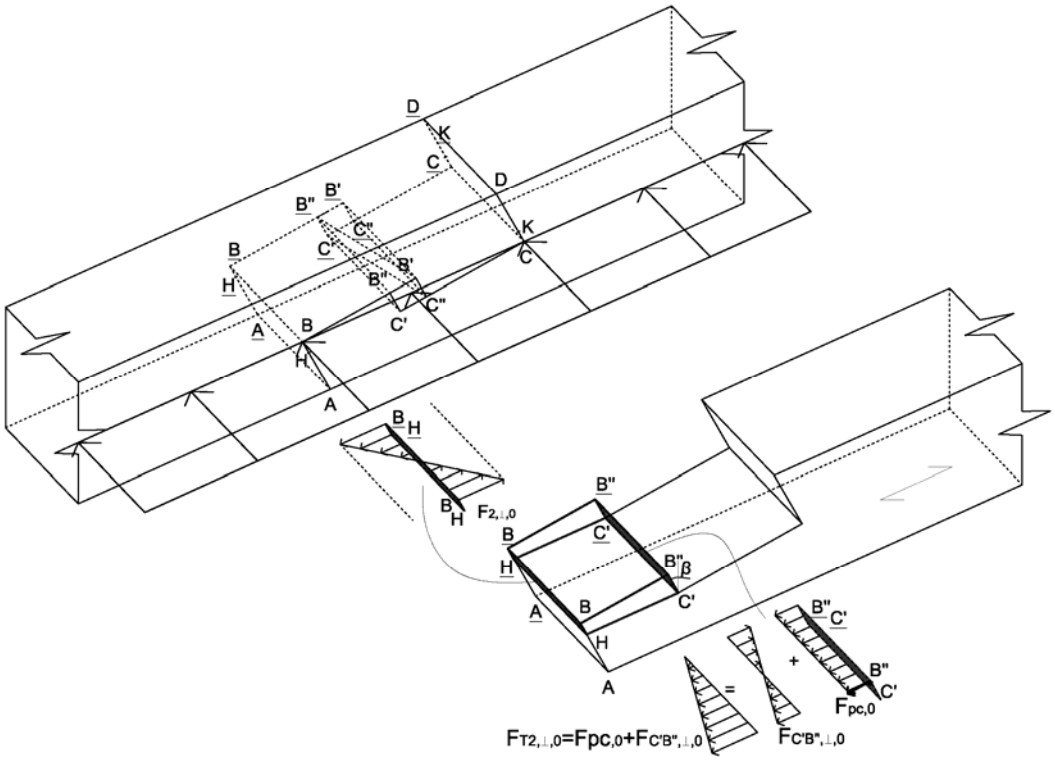

Figure 10: Upper specimen: three dimensional representation of the *Jupiter joint*s' specimen (loaded on the weak axis). Lower specimen: Complex mechanisms of transmission of the forces in the BB''C'HBB''C'H prism

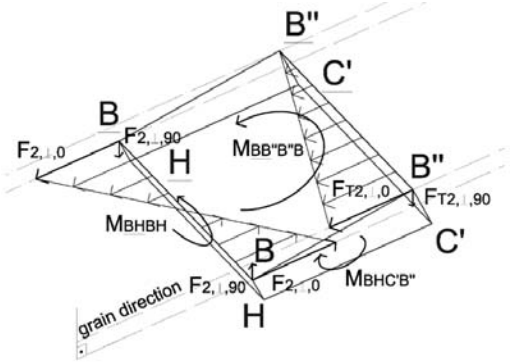

Figure 11: Detail of the forces in the BB''C'HBB''C'H prism and relative developed kinematic mechanisms

FM V: The shear failure is present both on the compressed and on the tension side. The shear mechanism develops even though on different shear planes.

Tension side: the shear plane $\overline{B'K}$. The shear failure can also verify on the tension side, on the fibers in $\overline{B'K}$, because of the compression on $\overline{CD}$ (specimen J60_5_w_F12, Figure 8 - c).

Compression side: the shear force acting on the shear plane $\overline{C'H}$ is described in equation (7) and depends on equation (8).

$$F_{v,2} = F_{2,\perp,0} - F_{T2,\perp,0} \tag{7}$$

$$F_{T2,\perp,0} = F_{pc,0} + F_{B''C',\perp,0} \tag{8}$$

where: $F_{C'B'',\perp}$ = resultant force on the $\overline{C'B''}$ surface due to the external load, perpendicular to the surface; $F_{T2,\perp}$ = resultant force on the table 2 (T2 = surface $\overline{C'B''}$) of the joint, perpendicular to the surface; $F_{2,\perp}$ = resultant force on the face $\overline{AB}$ due to the external applied load.

The section is verified when:

$$\frac{F_{v,2}}{b \cdot \overline{C'H}} \leq R_v \tag{9}$$

Referring to Figure 11, the mechanism is further completed with some observations about the kinematic mechanisms in the third dimension. Because of both different resultant forces at the two compression and tension side, the anticlockwise torque MB''B'BB'' forms on the shear plane (transversal direction).

As an example that demonstrates the failure mechanisms in the beam, some images from the tests of the failure of the specimen J60_5_w_F0 [12] are proposed in the Figure 12:

(a) The upper timber part is rotated respect to the lower timber part due to the torque MBHBH that creates a torsion along the beam's axis.

(b) The internal kinematic mechanisms (torque MBHC'B'') causes a rotation that brings to the further compression of the segment $\overline{BB'}$ on the tension side and (c) the segment $\overline{AB}$ on the compression side. The key is a further fixed point that establish a horizontal rotation axis that causes the torsion of the upper respect to the lower part.

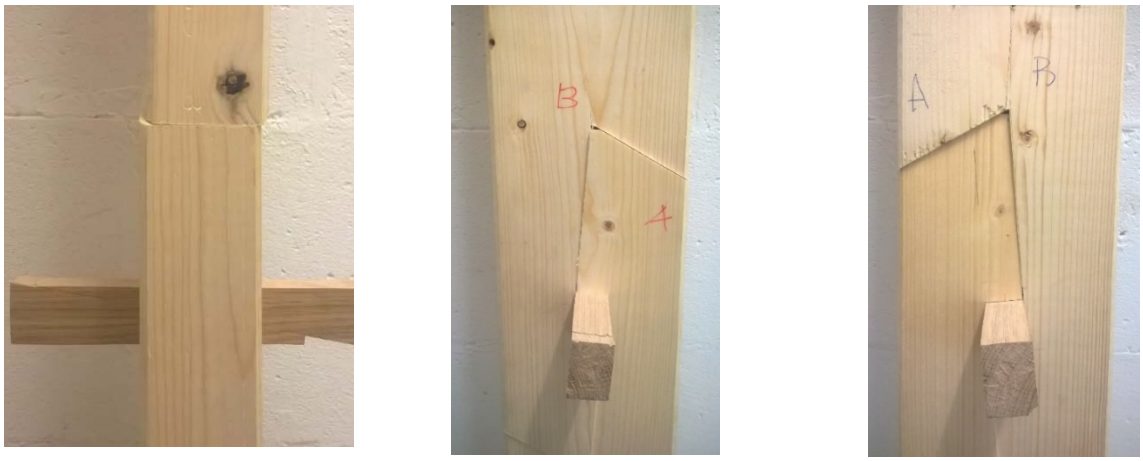

(a) (b) (c)

Figure 12: FM II on the specimen J60_5_w_F0 (a) Rotation of the upper to le lover side. The right part is compressed, the left is tensile-stressed. (b) Tension side. The segment BB' is further compressed. (c) Compression side. The segment BA is further compressed

4 EVALUATION OF THE ROTATIONAL STIFFNESS

Referring to Figure 13, the calculation of the rotational stiffness k_φ in equation (15), is done according to the ultimate values of applied load and the displacements of the correspondent piston P_{II}. The calculation is performed as follows.

$$e = 0.405m \tag{10}$$

$$M_u = \frac{F_{II,u}}{2} \cdot e \tag{11}$$

$$u_{PII}(M_u) \tag{12}$$

$$\theta_{[\deg]} = arctg\left(\frac{u_{P2}}{l_b/2}\right) \tag{13}$$

$$\theta_{[rad]} = \frac{\theta_{[\deg]} \cdot \pi}{180°} \tag{14}$$

$$k_\varphi = \frac{M_u}{\theta_{[rad]}} \tag{15}$$

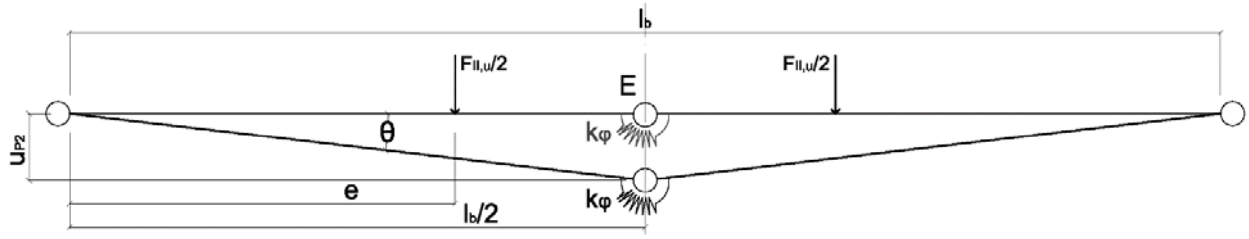

Figure 13: Scheme of the rotational stiffness of the hinge

The reference value of rotational stiffness for the *Jupiter joint* along both the strong and the weak axis is considered the rotational stiffness obtained in the pure bending tests, calculated according to equation (15). The tests of reference are the one performed in vertical position with the testing machine 2. The equation (16) gives a resume of the experimental values of rotational stiffness in the *Jupiter joint* for the strong and weak axis.

$$\begin{aligned} k\varphi y_{\exp} &= 663 \qquad (strong \quad axis) \\ k\varphi z_{\exp} &= 262 \qquad (weak \quad axis) \end{aligned} \tag{16}$$

5. GENERAL CONCLUSIONS ON THE *JUPITER JOINT*

5.1. Load-carrying capacity

The comparison of the tests of the *Jupiter joint* leads to the followings conclusions:

1. The load-carrying capacity of the *Jupiter joint* along both the strong and weak axis is the same for the specimens loaded in pure compression and in pure bending.
2. In pure compression, the test specimen loaded on the weak axis showed a smaller ultimate strength [*Fu*] respect to the one loaded on the strong axis. The reason of this difference in the load-carrying capacity of the specimen can rely in the specimen manufacturing, the timber's specific lower properties, and finally in the test asset.
3. The presence of imperfections in the test asset is a more significant factor for the specimen loaded on the weak axis; here, the minimum imperfection can really affect the test results.

5.2. Failure modes

The FM II. shear/tension perpendicular to the grain failure in the point B is the most recurrent, both on the weak and in the strong axis' tests. The basic reason of the failure is the same

concluded and calculated for the *halved undersquinted scarf* joint [12]; nevertheless, in the *Jupiter joint* the problem is more complex because of the presence of more factors:

1. the presence of imperfections (that affect the weak axis more than the strong axis);
2. the pre-compression F_{pc} of the key;
3. the entity of both the angle α of the squint and β of the splayed surface;
4. the internal friction (not considered in the present section of the work);

Furthermore, the FM V is dependent on the length of the shear segment $\overline{C'H}$. The bigger is the surface of the shear plane (longer shear segment), the bigger is the load-carrying capacity of the specimen.

REFERENCES

[1] Blass H. J., Aune P. et alii. (1995). Timber Engineering, *STEP 1 (STEP 2)*, *Basis of design, material properties, structural components and joints*, Centrum Hout, The Netherlands.

[2] Branco J. M., Descamps T. (2015). Analysis and strengthening of carpentry joints. in: *construction and building materials,* 97 (2015) 34–47.

[3] Collings G. (1992). Circular Work in Carpentry and Joinery, illustrated by Karl Shumaker, Roger Holmes, Canada.

[4] Fairham W., Roberts G. R. (1920). *Woodwork Joints: Carpentry, Joinery, Cabinet-Making*: The Woodworker Series, Ewan –Bros., London.

[5] Gatzelu L., D., (1899). *Carpinteria de armar*, Madrid.

[6] Gerner, M. (1983). *Fachwerk: Entwicklung, Gefüge, Instandsetzung*, Deutsche Verlags-Antstalt, Stuttgard.

[7] Gerner, M. (1992). *Handwerkliche Holzverbindungen für Zimmerer*, Deutsche Verlags-Antstalt, Stuttgard.

[8] Graubner W. (2004). *Holzverbindungen - Gegenüberstellungen japanischer und europäischer Lösungen*, Deutsche Verlags-Anstalt, München Stuttgard 2004.

[9] Gustafsson J., (ca. 1990). *A study of strenght of notched beams.* Division of Structural Mechanics, Lund Institute of Technology. Lund, Sweden

[10] Gustafsson P. (2003). *Fracture perpendicular to Grain – Structural applications*. In: Thelandersson and Larsen H., J., Timber Engineering, Wiley.

[11] Madsen B. (2000). *Behaviour of Timber Connections*. Vancouver, Canada: Timber engineering Ltd.

[12] Perria E. (2017). "*Characterization of halved undersquinted scarf joint and stop-splayed undersquinted & tabled scarf joint with key (Jupiter joint)"*. Dissertation submitted to the Department of Architecture, Civil Engineering and Environmental Sciences University of Braunschweig – Institute of Technology and the Department of Civil and Environmental Engineering University of Florence".

[13] Sobon J. A. (2002). *Historic American Timber Joinery: A Graphic Guide*, Pub. By Timber Framers Guild, Ed. by Kenneth Rower. Retrived from https://www.ncptt.nps.gov/wp-content/uploads/2004-08.pdf.

[14] Tregold, T., (1858). *Elementary principles of carpentry*, John Weale, London.